ACS APPLIED NANO MATERIALS

www.acsanm.org Article

Plasmonic Detection of Mercury via Amalgamation on Gold Nanorods Coated with PEG-Thiol

John R. Crockett, Hla Win-Piazza, Joseph E. Doebler, Tianqi Luan, and Ying Bao*

Cite This: *ACS Appl. Nano Mater.* 2021, 4, 1654−1663 Read Online

ACCESS | Metrics & More | Article Recommendations | Supporting Information

ABSTRACT: Gold nanorods (AuNRs) have emerged as a powerful element in the development of nanomaterial-based sensors due to their localized surface plasmon resonance extinction at visible and near-infrared wavelengths. In this study, we present a strategy for plasmonic detection of mercury using PEG-thiol-coated AuNRs (PEG@AuNRs). The PEG@AuNRs, prepared by a simple ligand exchange, demonstrate superior advantages including sensitivity, stability, and specificity than the as-synthesized hexadecyltrimethylammonium bromide-coated AuNRs. The plasmonic responses of PEG@AuNRs toward the same amount of Hg in the system can be significantly manipulated by adjusting the AuNR concentration in the system and the incubation time between AuNRs and Hg^{2+}. Both Hg^{2+}−S complexation and amalgam formation contribute to the unique behavior of plasmonic response which enable the design of a smart Hg^{2+}-sensing platform with an adjustable peak plasmonic response region. This study not only demonstrates the advantages of mercury-sensing systems based on PEG@AuNRs but also advances the fundamental understanding of ligand impacts on plasmonic properties for the plasmonic detection of mercury.

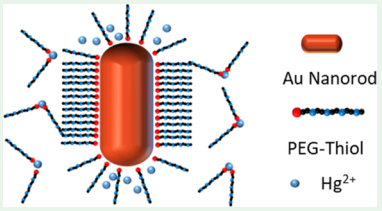

KEYWORDS: *gold nanorod, PEG-thiol ligand, plasmonic, amalgamation, mercury detection, Hg^{2+}−S complexation*

INTRODUCTION

Mercury, as one of the most toxic metals, is not biodegradable and can accumulate in living organisms, where even trace amounts can accrue to cause damage to the brain, kidneys, lungs, and the nervous system.[1−3] Mercury pollution, especially from the water-soluble divalent mercury ion (Hg^{2+}), which is one of the most stable inorganic forms, continues to be a serious issue of concern on the global scale.[4] Great efforts have been devoted to exploring various approaches for monitoring Hg^{2+} in aqueous samples. Currently, various techniques, including atomic fluorescence spectroscopy, gas chromatography−inductively coupled plasma mass spectrometry, atomic absorption spectrometry, and cold vapor mercury analysis, are available for the determination of Hg^{2+}.[5,6] However, these techniques are restricted by the cost of equipment, complexity of sample pre-treatment, and the necessity of a laboratory setting. Therefore, a highly sensitive and selective approach to detecting Hg^{2+} that avoids the need for advanced instruments is urgently needed.

Due to their sensitive optical response arising from localized surface plasmon resonance, novel metal nanomaterials have been frequently used to construct sensors for detecting Hg^{2+}.[7−9] Among the potential sensing techniques, the colorimetric method using metal nanomaterials for Hg^{2+} detection allows the analyte recognition event to be converted to naked-eye-sensitive color change and is often favored due to its simplicity, speed, and low cost.[10−14] In order to make the colorimetric detection of Hg^{2+} possible, many studies have applied the aggregation-based method, which relies on Hg^{2+} directly or indirectly changing the distance between metal nanoparticles resulting in a strong plasmon coupling of these metal nanoparticles and a color change in the colloidal solution. DNA, organic molecules, and peptides are functional ligands often used to detect Hg^{2+} using the aggregation method.[15−18] For example, mercapto derivatives with sulfhydryl group molecules often functionalize the surface of metal nanoparticles due to the strong Au/Ag−S bond. The introduction of Hg^{2+} will induce the aggregation of nanoparticles by forming interparticle complexes between Hg^{2+} and labeling ligands, which then lead to the color change.[19] However, there are intrinsic disadvantages in such methods, including unpredictable auto-aggregation and the necessity for labeling steps on the surface of nanoparticles.

To overcome these issues, the morphology transition-based method has been developed, which recognizes the target Hg^{2+} by inducing the surface chemical reaction of a certain analyte. Chen and co-workers demonstrated a novel sensor for Hg^{2+} detection based on the morphology transition of silver nanoprisms modified with thiol-ended ligands. In their system, the presence of thiol ligands can protect the stability of silver nanoprisms without Hg^{2+}. When Hg^{2+} is added, the thiol group

Received: November 24, 2020
Accepted: January 19, 2021
Published: January 28, 2021

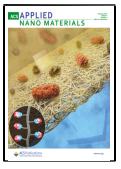

https://dx.doi.org/10.1021/acsanm.0c03134
ACS Appl. Nano Mater. 2021, 4, 1654−1663

detaches from the surface of silver nanoprisms forms complexes with Hg^{2+}, leading to the consumption of silver atoms on the surface by iodine. Eventually, the morphology of the particle is changed, which can be monitored by the color and UV−vis absorption spectra of the colloidal solution.[20] Xu and co-worker synthesized gold nanostars and used them as a probe for detecting Hg^{2+}. In this work, the morphology of gold nanostars was deformed due to the formation of Au−Hg amalgamate which changed the localized surface plasmonic resonance of gold nanostars.[21]

For high-sensitivity optical response based on morphology transition, gold nanorods (AuNRs) have shown their superior advantage over others due to their large spectral shift for a given change in their size, aspect ratio (AR), and refractive index of the surrounding media.[22−24] An early example using AuNRs for Hg^{2+} detection is from Rex et al. The detection was based on the amalgamation process between mercury and gold. The as-synthesized AuNRs were coated with hexadecyltrimethylammonium bromide (CTAB) ligands. The mercury formed by the reduction of Hg^{2+} initially deposited on the tips of AuNRs due to the low-density CTAB packing on the surface of AuNRs resulted in the decrease of the effective AR of the nanorods. The longitudinal band was highly sensitive to the AR change, which can be observed as a blue shift.[25] However, due to the nature of CTAB packing on AuNRs, it is known that the stability of CTAB-coated AuNRs (CTAB@AuNRs) is low, which is not ideal for a practical sensor.[22,26] A productive AuNR sensing system would ideally have stable NRs in a complex solution as well as have a preferred reaction location on the area of the NR surface that gives the most sensitive plasmonic response. Furthermore, it is advantageous for the region of maximum plasmonic response to be adjustable to the unknown Hg^{2+} concentration.

Herein, the PEG-thiol-coated AuNRs (PEG@AuNRs) were fabricated by a simple ligand-exchange approach and were used as plasmonic nanotransducers to monitor the amalgamation of Hg with the AuNRs. Due to the local curvature on the AuNR, the amalgamation occurred preferentially and actively at the rod tips of the PEG@AuNRs, which give the most sensitive plasmonic response. The PEG@AuNRs show superior performances, including sensitivity, stability and specificity, over the CTAB@AuNRs. Furthermore, by varying both the concentration of overall PEG@AuNRs and the incubation time ($t_{incubation}$) between PEG@AuNRs and Hg^{2+}, the amount of attached PEG-thiol ligands in the system was controlled, which in turn had an impact on the plasmonic responses of PEG@AuNRs to the same amount of Hg. The mechanism for the strategy based on PEG@AuNRs was proposed and established by the evidence provided via various techniques. We believe that the reported new strategy for the detection of Hg^{2+} is promising for constructing a smart Hg^{2+}-sensing platform with adjustable peak sensitivity and selectivity.

MATERIALS AND METHODS

Materials. CTAB, gold(III) chloride trihydrate ($HAuCl_4 \cdot 3H_2O$), L-ascorbic acid (L-AA), hydrochloric acid, thiolate polyethylene glycol (PEG-SH) (M_n 5000), and ethanol (EtOH) were purchased from Sigma-Aldrich (USA). Sodium borohydride ($NaBH_4$) was purchased from Merck, and silver nitrate ($AgNO_3$) was purchased from Fisher Scientific (USA). Mercury chloride was purchased from Sigma-Aldrich (USA). All chemicals were used as received without further purification.

Synthesis of CTAB@AuNRs. The CTAB@AuNRs were synthesized in a large batch via a seed-mediated growth method.[27] To prepare the seeds, 0.250 mL of 0.01 M $HAuCl_4$ was added to 10.0 mL of 0.1 M CTAB. 0.600 mL of 0.01 M $NaBH_4$ was then added. The solution color changed from orange to light brown, indicating the formation of gold seeds. The solution was stirred for 2 min and left to stand for 2 h. For the growth solution, 450 mL of 0.094 M CTAB aqueous solution was prepared and fully dissolved by putting it in a 45 °C water bath. The solution was cooled to room temperature (RT) before further use. 18 mL of 0.01 M $HAuCl_4$ was then added to the surfactant solution and fully mixed by inversion. This was followed by the addition of 2.7 mL of 0.01 M $AgNO_3$ and 2.9 mL of 0.1 M L-AA, and the solution was fully mixed by inversion. Finally, 1.8 mL of Au seed solution was added to the mixture and the solution was inverted for 30 s and then left in a dark cabinet at RT for approximately 12 h. Note that the as-synthesized CTAB@AuNRs were first purified by centrifugation twice at 18,000 rpm for 20 min in order to remove the redundant CTAB in solution and can then be used for detecting Hg^{2+}.

Ligand Exchange with PEG-Thiol. The as-synthesized 40 mL CTAB@AuNR solution was first purified by centrifugation twice at 18,000 rpm for 20 min and then re-dispersed in 40 mL nanopure water with 33 mg PEG-thiol, which was used to replace the CTAB layers on AuNRs. The solution was stirred at RT for 14 h before it was centrifuged four more times before use. It is important to note that during the first two times, the particles were redispersed in ethanol solvent and nanopure water was used as a solvent for the last two times. The final solution volume was 20 mL. The prepared solution was then stored under refrigeration until needed.

Detection Method. As a general procedure for detecting Hg^{2+}, 300 μL of PEG@AuNRs with a specific concentration was first mixed with different concentrations of 10 μL $HgCl_2$ solution. Depending on the $t_{incubation}$, 300 μL of fresh ice-cold $NaBH_4$ solution was subsequently added to the mixture. The ice-cold $NaBH_4$ solution was prepared by diluting 1 mL of 16.5 mM $NaBH_4$ solution with 9 mL of chilled water. The final solution was mixed vigorously and left for about 10−15 min at RT until the color of the solution changed completely. To ensure the completion of amalgamation, the solutions were kept at RT for 20 min before the measurement of the absorption spectrum. Experiments on detecting other metal ions were performed similarly. The concentration of AuNRs was determined by the absorption intensity of the longitudinal peak for the solution. The default absorption intensity of AuNR solution for sensing was about 0.6 abs. (with 1 cm path length).

Characterization. All UV−vis−NIR spectra for sensitivity and selectivity were recorded with a JASCO UV−Vis−NIR spectrometer. Scanning transmission electron microscopy (STEM) images of AuNRs were obtained using a JEOL 7200 scanning electron microscope in STEM mode. High-resolution transmission electron microscopy (HRTEM) images were acquired on a FEI Tecnai Spirit equipped with a Gatan Ultrascan 4000 4k × 4k CCD camera. Nuclear magnetic resonance (NMR) spectra were acquired on a FT-NMR—Bruker AVANCE III 500 MHz in ^1H NMR mode.

RESULTS AND DISCUSSION

Synthesis, PEG Ligand Modification, and Characterization. The PEG@AuNRs were prepared by mixing PEG-SH with CTAB@AuNRs. After the reaction of the thiol group of PEG with the surface of AuNRs for 14 h at RT, CTAB was removed by repeated washing and centrifugation with ethanol and water, as depicted in Figure 1a. The absorption spectra of AuNR solution before and after ligand exchange were measured (Figure 1b). The as-prepared CTAB@AuNR solution (blue line) has two absorption peaks at 510 and 770 nm that are assigned to the transverse localized surface plasmonic resonance (TSPR) and longitudinal localized surface plasmonic resonance (LSPR) bands of AuNRs, respectively. When functionalized with the PEG thiol ligand (red line), the SPR bands of PEG@AuNRs do not show obvious shifts (<5 nm), indicating that PEG@AuNRs were prepared without the formation of aggregates, and similar

https://dx.doi.org/10.1021/acsanm.0c03134
ACS Appl. Nano Mater. 2021, 4, 1654−1663

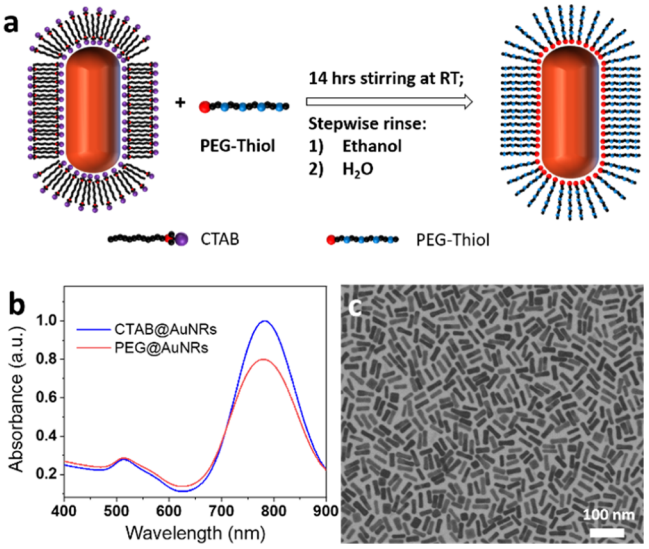

Figure 1. (a) Schematic illustration of the ligand-exchange process between PEG-thiol ligands and CTAB ligands on the surface of AuNRs. (b) UV−vis absorption spectra of CTAB@AuNRs and PEG@AuNRs. (c) STEM image of PEG@AuNRs after ligand exchange.

observations have been reported by others as well.[28] The as-synthesized CTAB@AuNRs and the ligand-exchanged PEG@AuNRs were characterized via NMR spectroscopy. Figure S1 and Table S1 show the ^{1}H NMR spectra of CTAB@AuNRs (a) and PEG@AuNRs (b) and the summary of ^{1}H chemical shift assignment for CTAB which have been reported previously.[29,30] Comparing the ^{1}H NMR spectrum of CTAB@AuNRs, it is clear that the ^{1}H NMR spectrum of PEG@AuNRs (after the ligand-exchange process) shows significant disappearance of the CTAB methyl resonance at 0.85 ppm (red dashed circle), and the presence of PEG long chain resonance at 3.5 ppm is clearly distinguishable. These NMR results demonstrate that the ligand-exchange process can significantly replace CTAB with PEG. STEM analysis confirmed that the PEG@AuNRs remained well-dispersed after the ligand exchange. The STEM images of CTAB@AuNRs and PEG@AuNRs in Figures S2 and 1c show that the morphology of AuNRs is not impacted during the ligand exchange and the majority of nanomaterials have a rod shape, with a small number of cubes produced as well. In addition, from the STEM image, the length and the width of the synthesized AuNRs were around 48 ± 5 and 14 ± 2 nm, respectively, with an AR of 3.6 ± 0.8. It is noticed that the process of ligand exchange decreases the AuNR concentration to some extent. Thus, in this study, the LSPR absorption intensity of AuNR solution will be used to represent the concentration of AuNRs in the sensing system.

Comparison of Sensitivity, Selectivity, and Stability of PEG@AuNRs and CTAB@AuNRs in Mercury Sensing. The performances of CTAB@AuNRs and PEG@AuNRs in detecting mercury were compared. The mercury-sensing mechanism for both cases is based on the amalgamation process. To trigger this amalgamation process, fresh, ice-cold $NaBH_4$ was employed to reduce Hg^{2+} to Hg^0. Then, the Hg^0 diffused on the surface of AuNRs, where it subsequently underwent amalgamation with the AuNRs. It is important to know that most of the active sites of the AuNRs were located at their tips,[25,31] where the amalgams formed more efficiently, since the ligands in the tips are relatively loose due to their positive curvature. Therefore, the long axis of the AuNR decreases more drastically due to amalgamation than the short axis, resulting in a reduced AR. On the absorption spectra, this will cause the LSPR to have a blue shift due to the two concomitant effects resulting from the deposition of mercury: alteration of the nanorod surface composition and shape transition. Based on the relationship between LSPR shifts and the concentration of Hg^{2+} ($[Hg^{2+}]$), a detection system for Hg^{2+} can be built.

The initial absorption intensities of both CTAB@AuNR and PEG@AuNR systems are very similar, at about 0.62 abs., indicating the very similar concentration of AuNRs in the solutions. As shown in Figures 2a and S3, for both CTAB@

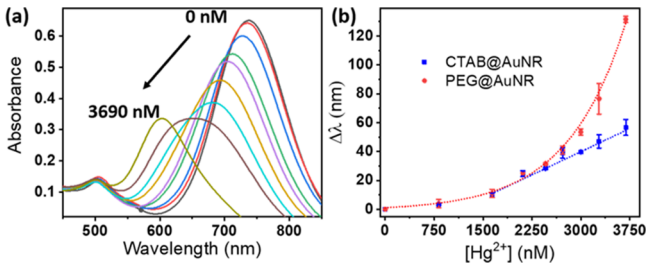

Figure 2. (a) Spectra of PEG@AuNRs amalgamated at various concentrations of Hg^{2+}: 0 nM (black), 820 nM (red), 1640 nM (blue), 1900 nM (green), 2460 nM (purple), 2720 nM (orange), 3000 nM (aquamarine), 3280 nM (brown) and 3690 nM (gold). (b) Plots of the mean of LSPR shifts for PEG@AuNR and CTAB@AuNR as a function of concentration of Hg^{2+}.

AuNRs and PEG@AuNRs, with the increase of $[Hg^{2+}]$ ranging from 0 up to 3690 nM, the LSPR peak shows a continuous blue shift (shorter wavelengths), while the TSPR peak is almost fixed at ∼510 nm. Thus, the degree of LSPR shift was used as the response to detect $[Hg^{2+}]$. It is worth mentioning that in these experiments, AuNR samples were all immersed in Hg^{2+} for less than 1 min before fresh ice-cold $NaBH_4$ solution was added, and all results were recorded after 10−15 min when the optical responses of the resulting AuNR solution were stable. The spectra at 0 nM Hg^{2+} for both CTAB@AuNRs and PEG@AuNRs were measured from the AuNRs mixed with $NaBH_4$, which result in a blue-shifted LSPR. From the collected spectra over the range of $[Hg^{2+}]$, the LSPR peak of CTAB@AuNRs started at 750 nm with 0 nM Hg^{2+} and shifted to 695 nm at 3690 nM Hg^{2+}. In contrast, the PEG@AuNR solution shows a larger shift range, from 780 nm with 0 nM Hg^{2+} to 600 nm at 3960 nM Hg^{2+}.

Figure 2b summarizes the mean of the LSPR shift of the CTAB@AuNR solution (blue line) and the PEG@AuNR solution (red line) based on three trials as a function of $[Hg^{2+}]$ for each system. $\Delta\lambda$ is defined as the LSPR wavelength change relative to its corresponding initial reference value (at 0 mM Hg^{2+}). At lower concentrations ranging from 0 to 1640 nM, the optical responses for both CTAB@AuNRs and PEG@AuNRs are linear. However, as $[Hg^{2+}]$ increases, the optical responses of the CTAB@AuNR and PEG@AuNR systems show an interesting deviation. For the CTAB@AuNR system, a linear response with R^2 = 0.987 was obtained for measurements performed in the 1640−3690 nM Hg^{2+} range. In comparison, the PEG@AuNR system shows an exponential change (R^2 = 0.993) as a function of $[Hg^{2+}]$, demonstrating a much higher sensitivity to changes in this $[Hg^{2+}]$ range. Note

https://dx.doi.org/10.1021/acsanm.0c03134
ACS Appl. Nano Mater. 2021, 4, 1654−1663

that at higher concentrations (>3690 nM), the $\Delta\lambda$ reaches a plateau and barely changes, which will be discussed further later. Thus, the AuNRs exhibit a disparate performance with different ligands, suggesting the vital role of these ligands in sensing systems.

One distinct difference between CTAB@AuNRs and PEG@AuNRs is that the surface of AuNRs has a double layer of CTAB or a single layer of PEG, respectively, as shown in Figure 1a. It is possible that this difference in the density of ligands around the AuNRs has an impact on their relative detecting performance due to unequal accessibility. The ligands around the surface of AuNRs impede Hg^0 from accessing the surface, and the ligand density is higher for CTAB@AuNRs. Additionally, there must be a certain number of free CTAB molecules in the CTAB@AuNR colloidal solution as the outer layer of the CTAB bilayer must continuously exchange dynamically in order to stabilize the AuNRs.[22] It is possible that the surface of AuNRs is covered by ligands even as the amalgamation process disrupts the initial packed ligands on the AuNR surface. Thus, the optical response of CTAB@AuNRs is linear to additional $[Hg^{2+}]$. However, in the case of PEG@AuNR solution, the density of PEG around the AuNR surface is lower than that with CTAB due to the single layer. Thus, the contact area between mercury and the gold surface is larger, resulting in significantly higher amalgamation rates as reported elsewhere.[32] With higher concentrations of additional Hg^{2+}, there is a larger extent of amalgamation reactions resulting in a larger optical response of AuNRs.

Figure 3a shows the images of PEG@AuNR (top) and CTAB@AuNR (bottom) solutions after reacting with the same

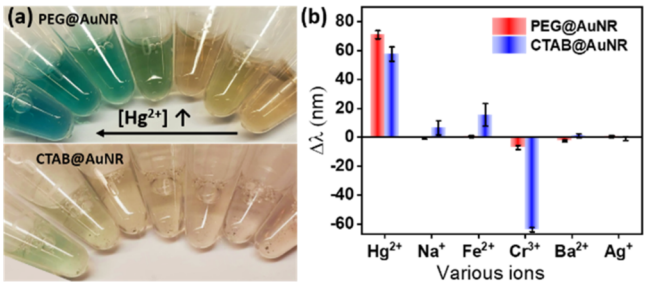

Figure 3. (a) Images of AuNR solutions after reduction with mercury, PEG@AuNRs (top) and CTAB@AuNRs (bottom). Concentration of Hg^{2+} from right to left in each tubes are as follows: 0, 820, 1640, 1900, 2460, 2720, and 3280 nM. (b) Selectivity of CTAB@AuNRs and PEG@AuNRs against indicated ions (whose concentration is 3280 nM).

range of $[Hg^{2+}]$, showing the transition of the solutions' color from red (right, low $[Hg^{2+}]$) toward green (left, high $[Hg^{2+}]$), which well-correlated with the observed spectral change seen in Figure 2a. These photos were taken one day after the reaction was complete. The PEG@AuNR system solutions have clear differences in color, are still very well dispersed, and have no aggregation formed, while the CTAB@AuNR system solutions formed aggregates which precipitated out of the solution leaving the solution colors very pale. These results are not surprising since it is well known that PEG-modified AuNRs are more stable under various conditions than CTAB-modified AuNRs, as claimed in other studies.[28,33]

To further study the specificity performance of CTAB@AuNRs and PEG@AuNRs for the determination of Hg^{2+}, some inorganic metal ions were tested under the same experimental conditions, including Ag^+, Ba^{2+}, Cr^{3+}, Fe^{2+}, and Na^+. The inorganic metal ions selected for use in this paper are commonly used in the literature as interference ions and were chosen to be consistent with related works.[21,34] The same amount of CTAB@AuNRs and PEG@AuNRs was exposed to 3280 nM solutions of each of those metal ions as well as to Hg^{2+} and 0.8 mM $NaBH_4$ solution was then added. The results are shown in Figure 3b. Each column represents the $\Delta\lambda$ averaged over three trials. Note that the added ions were mixed with AuNRs for less than 1 min before adding $NaBH_4$. In the sensing system of PEG@AuNRs (red bar), the addition of Hg^{2+} causes a large shift of 71 nm, while there are no obvious shifts in the presence of other metal ions. This indicates the high selectivity against Hg^{2+} making PEG@AuNRs reliable for the determination of Hg^{2+} in complex samples.

We observed that the CTAB@AuNR system exhibits a dramatic shift to several metal ions. It is not surprising that the system has the largest blue shift, of about 57 nm, for Hg^{2+} due to the amalgamation-caused morphology change of AuNRs. Additionally, the LSPR of CTAB@AuNRs has a similar-sized red shift, about −64 nm, for Cr^{3+}. This is possible because Cr^{3+} can coordinate with nitrogen in the CTAB-capping ligand on AuNRs, inducing the aggregation of AuNRs, resulting in a significant red shift. Further evidence of this is that the corresponding solution of CTAB@AuNRs turns purple after mixing with Cr^{3+}, indicating the aggregation of AuNRs. Furthermore, it is noteworthy that the standard deviations of $\Delta\lambda$ shifts in the CTAB@AuNR system are much larger than those in the PEG@AuNR system, particularly for Hg^{2+}, Na^+, and Fe^{2+}. We believe that the amount of free CTAB in the CTAB@AuNR solution will have an impact on the reproducibility of each trial, and it is challenging to obtain accurate concentrations of CTAB based on standard procedures. The standard procedure of washing the synthesized CTAB@AuNRs two times maintains the CTAB concentration under 0.01 mM but does not allow for more precise control.[22,35]

Manipulating the Mercury-Sensing Performance of PEG@GNRs. *Dilution Impact.* Various concentrations of PEG@AuNRs, determined by the LSPR absorption intensity of the solution, were prepared via dilution or concentration processes to study the rates of LSPR shift in a range of $[Hg^{2+}]$ and the results are shown in Figure 4a. The maximum $\Delta\lambda$ for

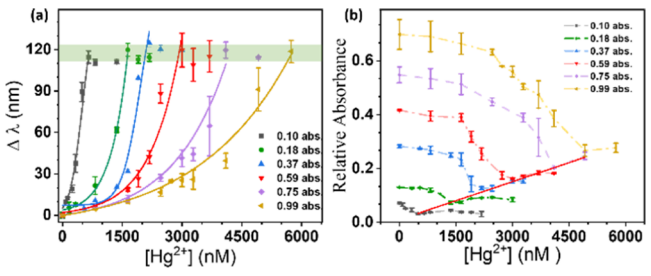

Figure 4. (a) Plots of mean LSPR shifts of PEG@AuNRs with various concentrations of solutions as the function of $[Hg^{2+}]$. Curves in (a) fitted to data before plateau (green shaded area) are reached. (b) Plots of the mean of relative absorbance of PEG@AuNR solutions against various $[Hg^{2+}]$. The value of relative absorbance is obtained by subtracting the TSPR absorption intensity from the LSPR absorption intensity of the spectrum. The red curve is the linear fitting of the lowest point on each absorption solution.

https://dx.doi.org/10.1021/acsanm.0c03134
ACS Appl. Nano Mater. 2021, 4, 1654−1663

all systems were similar, which we call the plateau. The approximate plateau is shown in green shading in Figure 4a. The result for the PEG@AuNRs with 0.99 abs., plotted in yellow in Figure 4a, shows that the mean of $\Delta\lambda$ follows an exponential increase (R^2 = 0.99) as the function of [Hg^{2+}] grows from 0 to 5747 nM. When the concentration of AuNRs decreases to an absorption of 0.75 abs., the mean of $\Delta\lambda$ similarly follows an exponential increase as a function of [Hg^{2+}], though this increase is faster than before and the plateau is reached around 4100 nM, as is shown in purple in Figure 4a. With further dilution of AuNR concentration, the rate of change continues to have an exponential relationship with [Hg^{2+}], though the growth rate is faster, and the plateau is reached at increasingly low levels of [Hg^{2+}]. Note that the curves in Figure 4a were only fitted to data before the plateau was reached for each system in order to clearly illustrate the relationships between [Hg^{2+}] and $\Delta\lambda$ in the regions where $\Delta\lambda$ is changing. Figure 4 indicates that a region of high sensitivity to changes in [Hg^{2+}] can be selected by adjusting the concentration of AuNRs appropriately. The reason for $\Delta\lambda$ reaching its "plateau" quicker when the AuNR concentration is lower was mentioned above. With lower concentrations of AuNRs but the same amount of Hg^{2+}, there will be more amalgamation of each individual nanorod. The consistent maximum $\Delta\lambda$ ("plateau") indicates that the final shape of individual AuNRs due to the impact of amalgamation is the same regardless of the concentration of AuNRs in solution if [Hg^{2+}] is sufficiently high. In addition, the detection limit of each concentration of PEG@AuNRs was calculated based on the equation LOD = 3S_blank/slope. The results are summarized in Table S2. It is worth mentioning that the blank solutions were obtained by mixing the PEG@AuNR solutions with certain concentrations and the sodium borohydride solution. Overall, the LOD is not much different when changing the NR concentration and there is no trend in LOD changes when increasing the PEG@AuNR concentration.

Figure 4b shows the mean difference in relative absorption intensity of amalgamated PEG@AuNR solutions at various [Hg^{2+}], obtained by subtracting the TSPR absorption intensity from the LSPR absorption intensity of the spectra. This relationship is obtained for systems with differing concentrations of AuNR solution. Each system's results are individually plotted in Figure S4. In general, the trend for each system is similar. When [Hg^{2+}] is increased, the difference in TSPR/LSPR absorption intensity initially decreases and then reaches a turning point, which again begins to increase as [Hg^{2+}] is increased further. The turning point for each system can be more clearly observed in the individual plots in Figure S4. We believe that during amalgamation, which is the process of Hg^0 diffusing into the AuNRs and forming Au@Hg nanoalloys, there are two key stages impacting the absorption intensity change. In the early stage, the amalgamation takes place more effectively and preferentially on the tips of the AuNRs, decreasing the AR of the AuNRs and causing the reduced difference in absorption intensity. This is likely due to the smaller scattering cross section of Au@Hg nanoalloys. In the later stage, the Hg^0 atoms continuously diffuse into the AuNRs, referred to as the "swelling effect",[36] driven by the difference in the cohesive energy between Hg (0.67 eV/atom) and Au (3.81 eV/atom). Thus, the size of Au@Hg nanoalloys gradually increases, leading to increased absorption intensity. Interestingly, the turning point for each case, when combined in one plot has a linear relationship (R^2 = 0.99), as shown in Figure 4b (red line). This linear fitting is useful in terms of predicting the turning point in any system with different AuNR concentrations.

Incubation Impact: Sensitivity and Specificity. The mercury-sensing performance was further manipulated by incubating the PEG@AuNRs with [Hg^{2+}] for different durations of time before adding $NaBH_4$. The hypothesis here was that the incubation process changes the density of PEG on the surface of AuNRs due to the complexation of thiol group and Hg^{2+} which impacts the amount of surface of AuNRs exposed to the external environment and eventually impacts the efficiency of amalgamation.

Figure 5a plots the results of the mean of $\Delta\lambda$ for PEG@AuNRs with different $t_{incubation}$ as the function of concentration

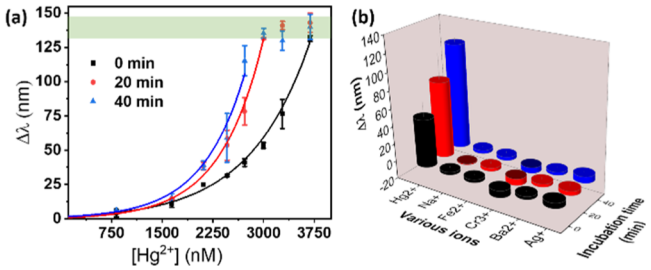

Figure 5. (a) Plots of $\Delta\lambda$ of PEG@AuNRs against the [Hg^{2+}] concentration with 0, 20, and 40 min of incubation times based on three trials. Curves in (a) fitted to data before plateau (green shaded area) is reached. (b) A comparison of the selectivity of PEG@AuNRs incubated with Hg^{2+}, Na^+, Fe^{2+}, Cr^{3+}, Ba^{2+}, and Ag^+ for 0, 20, and 4 min. (All at concentrations of 2720 nM.)

of Hg^{2+}. It clearly reveals that for the same concentration of PEG@AuNRs, with a longer $t_{incubation}$, $\Delta\lambda$ is higher for the same level of [Hg^{2+}] and the plateau is reached more quickly. Specifically, the PEG@AuNRs with 0 min of $t_{incubation}$ show an exponential growth (R^2 = 0.99) and do not show a $\Delta\lambda$ plateau in the [Hg^{2+}] range of 0−3690 nM. The PEG@AuNRs with 20 min of $t_{incubation}$ show an exponential increase of $\Delta\lambda$ (R^2 = 0.99) in the [Hg^{2+}] range of 0−3000 nM, reaching the plateau and not changing as [Hg^{2+}] is increased further from 3000 to 3690 nM. For 40 min of $t_{incubation}$, the [Hg^{2+}] range where $\Delta\lambda$ increases to the $\Delta\lambda$ plateau is even narrower (0−2720 nM). This result reveals that $t_{incubation}$ can improve the PEG@AuNR system's sensitivity performance.

The impact of incubation on the specificity of the PEG@AuNR system toward Hg^{2+} was also examined. We performed experiments to test the influence of the LSPR in the presence of other inorganic ions that were used in Figure 5b, including Ag^+, Ba^{2+}, Cr^{3+}, Fe^{2+}, and Na^+. Each column, as shown in Figure 5b, represents the $\Delta\lambda$ averaged over three trials, and from the results, only Hg^{2+} caused a significant $\Delta\lambda$, with the other metal ions showing small changes in three cases with various $t_{incubation}$. Among the three cases, the case with 40 min of $t_{incubation}$ shows the highest value of $\Delta\lambda$, about 120 nm, demonstrating the best specificity to Hg^{2+}, while there was a 40 nm change for the case with 0 min of $t_{incubation}$ and an 80 nm change for the case with 20 min of $t_{incubation}$. This implies that the $t_{incubation}$ can increase the specificity to Hg^{2+} while retaining low or no impact from other metal ions.

To understand the impact of incubation on the degree of deformation for AuNR morphology at various [Hg^{2+}], STEM

https://dx.doi.org/10.1021/acsanm.0c03134
ACS Appl. Nano Mater. 2021, 4, 1654−1663

was used to characterize the morphologies of PEG@AuNRs after reaction for systems with 0 and 40 min of $t_{incubation}$. The representative STEM images (Figure S5) show the rod shape for both systems with various $[Hg^{2+}]$. The changes in AR values from increasing the $[Hg^{2+}]$ for two systems are summarized in Figure 6a. The data in black represent the

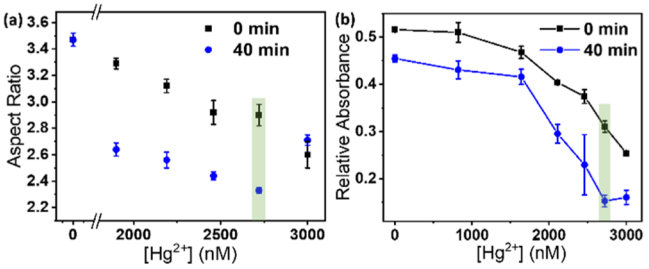

Figure 6. (a) The mean of AR value of amalgamated PEG@AuNRs against various $[Hg^{2+}]$. (b) The mean of relative absorption intensity of PEG@AuNR solution at various $[Hg^{2+}]$. The value of relative absorbance is obtained by subtracting the TSPR absorption intensity from the LSPR absorption intensity of the spectrum. Green shadow highlights the results for (a,b) at 3000 nM $[Hg^{2+}]$ condition.

AR of the amalgamated PEG@AuNRs from the system where PEG@AuNRs were incubated with Hg^{2+} for 0 min before reduction and subsequent amalgamation, while the data in blue represent the AR of AuNRs from the system where PEG@AuNRs were incubated with Hg^{2+} for 40 min before reduction and subsequent amalgamation.

When the system has 0 nM Hg^{2+}, $t_{incubation}$ does not impact AR. However, when introducing various amounts of Hg^{2+}, reduced to Hg for amalgamation, the AR values for each system are significantly different. For the system with 0 min of $t_{incubation}$, the AR continuously decreases from 3.47 ± 0.05 to 2.6 ± 0.1, as $[Hg^{2+}]$ is increased from 0 to 3000 nM, while for the system with 40 min of $t_{incubation}$, the AR value decreases from 3.47 ± 0.05 to 2.33 ± 0.02 when increasing $[Hg^{2+}]$ from 0 to 2720 nM but then increases to 2.71 ± 0.04 as $[Hg^{2+}]$ is increased to 3000 nM.

The process of morphology change was discussed earlier in the context of absorption intensity change at different $[Hg^{2+}]$, including the initial stage of reducing the AR of AuNRs and the later stage of gradual size increase due to the diffusion of Hg atoms to the AuNR, referred to as the "swelling effect". We believe that using the system with 0 min incubation, the range of $[Hg^{2+}]$ used was not large enough to reach the later stage where the AR increases with increasing $[Hg^{2+}]$. For the system with 40 min incubation, increasing $[Hg^{2+}]$ from 0 to 2720 nM results in a much larger AR decrease than the system with 0 min incubation and then reached the "swelling effect" stage at 3000 nM $[Hg^{2+}]$, where the AR begins increasing as $[Hg^{2+}]$ increases.

To provide additional evidence for the presence of "swelling effect", the mean difference in absorption intensity (obtained by taking the difference of the spectrum's LSPR and TSPR) for amalgamated PEG@AuNRs solutions against various $[Hg^{2+}]$ is plotted in Figure 6b. For the system with 0 min incubation (black color), the absorption intensity decreases over the range of Hg^{2+} which is consistent with the decrease of AR. For the system with 40 min incubation (blue color), the absorption intensity decreased initially and then increased starting from $[Hg^{2+}]$ at 2760 nM. At 3000 nM $[Hg^{2+}]$, the absorption intensity increases which matches the change of AR in Figure 4. The green shadow highlights the results obtained for both systems at 2760 nM $[Hg^{2+}]$ condition.

There are reported works using the AuNR solution-based localized surface plasmon resonance for mercury detection. The detection methods include amalgamation,[25,37,38] aggregation,[39,40] and surface-enhanced Raman scattering (SERS).[41,42] Those reported methods have various advantages such as high selectivity and sensitivity. However, there are intrinsic disadvantages to these approaches as well. The reported methods based on amalgamation often use CTAB@AuNRs which have a poor stability.[25,37,38] Aggregation-based methods are sensitive to ionic interference, and the sensing method is highly complex.[39,40] The SERS-based detection requires expensive and delicate equipment.[41,42] Our method does not have those drawbacks and is highly stable with straightforward preparation and detection. In addition, our method provides a broad linear range by changing the concentration of AuNRs or incubation time. See Table S3 for a more specific list of advantages and disadvantages of different types of detection methods.

Mechanism. *Proposed Model.* Figure 7 shows models of the final morphology of PEG@AuNRs after amalgamation at

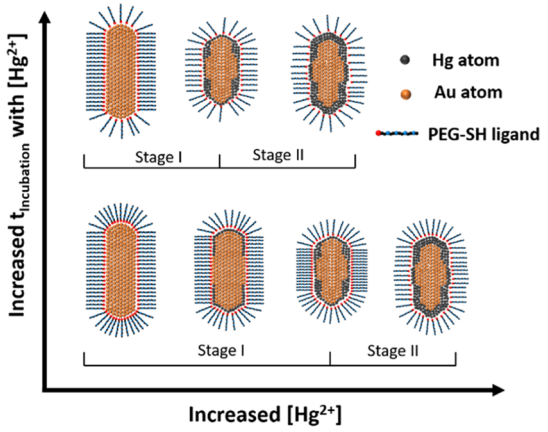

Figure 7. Illustration of the final morphology of PEG@AuNRs after amalgamation at various values of $t_{incubation}$ and $[Hg^{2+}]$ (not to scale). The following two stages will appear as Hg^{2+} concentration increases. Stage I: diffusion of Hg atoms into AuNRs, shortening or rounding the particle; stage II: diffusion of Hg atoms into AuNRs, gradually increasing the size due to an increase in the number of atoms per cluster. With more ligands on the surface of AuNRs, the amalgamated PEG@AuNRs will stay in stage I through higher $[Hg^{2+}]$.

various values of $t_{incubation}$ and $[Hg^{2+}]$. As depicted in the bottom row of the figure, in the case of low $t_{incubation}$ (such as 0 min), as the $[Hg^{2+}]$ increases, the morphology of the AuNRs moves from the first stage where the AR of the AuNRs is reduced because of amalgamation on the tips of the rods to a second stage of gradual size increases due to the continuous diffusion of Hg atoms into the AuNRs, leading to increasing number of atoms per cluster.[32,43] With additional incubation time, the ligand density on the AuNRs will be decreased due to detachment of the thiol group by Hg^{2+}. It is well known that an exceptionally strong complex can be formed between Hg^{2+} and sulfur (−S) or thiol (−SH) functional groups.[44−46] The stability constants (log K_f), an equilibrium constant for the formation of a complex in solution, are often used to measure the strength of the interaction between a metal ion and a

https://dx.doi.org/10.1021/acsanm.0c03134
ACS Appl. Nano Mater. 2021, 4, 1654−1663

ligand. It is reported that the log K_f of Hg(SCN)N is about 22, which is larger than that of Au(SCN)N.[47] −SCN is similar to −SH in that it can bind strongly onto the surface of the Au nanomaterial.[48,49] Thus, it is reasonable to propose that PEG-thiol, which was initially chemisorbed on the surface of AuNRs, will be partially removed and complexed with Hg^{2+}. Due to the high-energy surfaces on the tip (curved part) of the AuNRs, PEG-thiol on those locations will be removed first. The first model in both rows in Figure 7 indicates the PEG@AuNRs after incubation for a certain amount of time. The model in the top row has less PEG-thiol on the tip compared to the model in the bottom row due to the longer incubation time. With less PEG-thiol on the tip, this increases the accessibility of free Hg^{2+} (not complexed with the thiol group) to the surface of AuNRs and results in a significantly higher amalgamation rate. As shown in Figure 7, the more the PEG-thiol ligands are removed from AuNRs through increased $t_{incubation}$, the higher the degree of amalgamation process will happen at any given $[Hg^{2+}]$, causing additional reduction of the AuNR AR, which is then reflected in a higher sensitivity of AuNR. It also results in a faster transition from stage one to stage two for the same range of $[Hg^{2+}]$, as indicated by comparing the top and bottom rows of Figure 7 for any amount of $[Hg^{2+}]$.

Electron Microscopy. To investigate the interactions of Hg^{2+} and PEG@AuNRs, especially to understand the impact of the removal of PEG-thiol on the crystalline structure of AuNRs, PEG@AuNRs with and without Hg^{2+} incubation were characterized by HRTEM. As shown in Figure 8a, the PEG@AuNRs without Hg^{2+} incubation exhibit a highly consistent lattice fringe, indicating their monocrystalline structure. The lattice spacing distance of ~0.205/0.204 nm throughout the AuNRs corresponds to the (200) facet of gold materials, consistent with other reports.[50] With Hg^{2+} incubation for 40 min, the lattice spacings for (200) planes at the tip and near the curved edge were slightly increased to 0.212 nm, as indicated in Figure 8b, which should be attributed to the Au−SH bond being broken by the Hg^{2+}. Such lattice distortion is likely attributable to the fluctuation of surface ligands, and similar observations have been reported elsewhere.[51−53] In addition, due to the higher activity levels, such interactions selectively occur at the edge and tips of the AuNRs, facilitating higher sensitivity for Hg^{2+} detection.

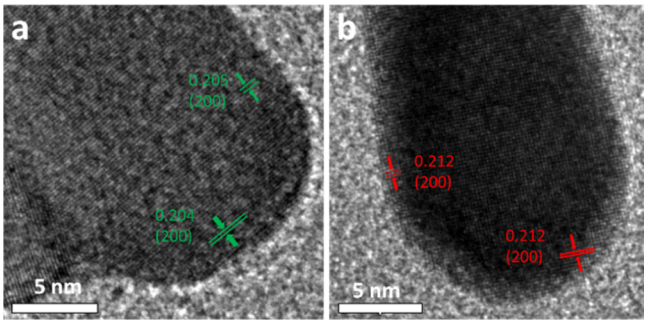

Figure 8. HRTEM images of (a) PEG@AuNRs without incubation and (b) PEG@AuNRs incubated with 1640 nM Hg^{2+} for 40 min.

Nuclear Magnetic Resonance. NMR spectroscopy is widely used to study the surface chemistry of gold nanoparticles.[54,55] In this work, we used NMR techniques to characterize the complexation between Hg^{2+} and PEG-SH removed from the surface of PEG@AuNRs. The NMR sample of PEG@AuNRs was washed with water and titrated with $HgCl_2$ to determine the ability of PEG to adsorb onto $HgCl_2$. Figure 9 shows the ^{1}H NMR spectra of free PEG-thiol ligands (20.2 mg), PEG@AuNRs, $HgCl_2$−PEG* solution, and $HgCl_2$−PEG# solution in DMSO-d_6. Table S3 contains the summary of ^{1}H NMR spectral assignments. It is worth mentioning that prior to the NMR spectral acquisitions, all PEG@AuNR samples were washed twice with ethanol, twice with water, and once with DMSO-d_6, and then redispersed into DMSO-d_6 in order to remove excess or nonbonded ligands in the solution. The $HgCl_2$−PEG* solution was the supernatant of a mixture of 1.1 mg of $HgCl_2$ and PEG@AuNR (with 5 times higher concentration than in the synthesized solution) which was mixed overnight. As shown in Figure S6, after incubating $HgCl_2$ and PEG@AuNR overnight, the mixture solution changes from a well-dispersed brownish red color (Figure S6a) to transparent with precipitates formed at the bottom (Figure S6b), indicating the detachment of PEG-thiol ligands from the AuNRs causing the precipitation of AuNRs. The mixture solution was then centrifuged and the supernatant $HgCl_2$−PEG* was used for ^{1}H NMR analysis. $HgCl_2$−PEG# solution was made from mixing 2.0 mg of $HgCl_2$ and free PEG (43.15 mg).

The ^{1}H NMR spectrum and chemical-shift assignments of free PEG-thiol ligands are shown in Figure 9a and the first column of Table S4. The ^{1}H NMR spectrum of PEG@AuNRs in Figure 9b and that expanded in Figure S7a,b, show the disappearance of methylene proton at 3.58 ppm and a slight line-broadening of the α-CH_2 proton adjacent to thiol (Table S4). This result indicates that PEG-thiol chains are stabilized on the surface of the AuNRs.[56−58]

To understand the interaction of PEG@AuNRs with $HgCl_2$, the supernatant of $HgCl_2$−PEG*was analyzed with ^{1}H NMR. Figure 9c shows the disappearance of proton resonance at 2.38, 2.64, 3.42, and 3.58 ppm. In the expanded Figure S7, the −SH proton shifted slightly downfield with a doublet (Figure S7C) instead of a triplet (as seen in Figure 9a,b at 2.26 ppm), and the methyl proton at 3.24 ppm showed reduced intensities, while the CH_2 quartet at 3.21 ppm collapsed to a singlet at 3.17 ppm [Figure S7B(c)]. Note that signals at 3.37 and 3.43 ppm are buried under residual HDO. These results indicate that there are no free PEG-thiol ligands in the $HgCl_2$−PEG* solution, and the changes in proton resonances are characteristics of ligands bound to metals or nanoparticles.[55] It is noteworthy that the CH_2 proton at position "e" of the PEG-thiol long chain shifted downfield, 4.04 ppm, with the ABq spin system. It is possible that the metal core, Hg^{2+}, can induce diastereotopicity in the methylene proton. This phenomenon has been reported in several articles.[59−61]

To further demonstrate the complexation of PEG thiol and Hg^{2+}, we explored the interaction between free PEG thiols and native $HgCl_2$ (shown in Figure 9d). The NMR sample ($HgCl_2$−PEG$^{\#}$) is prepared by mixing free PEG thiols with native $HgCl_2$ in DMSO-d_6 solvent for 6 h at RT. Compared to the ^{1}H NMR spectra of free PEG and PEG@AuNRs in Figure 9 and Table S3, the spectrum of $HgCl_2$−PEG$^{\#}$ showed a chemical shift variation with significant line broadening attributed to the complexation of PEG-thiol and Hg^{2+}. These results further demonstrate the formation of Hg^{2+} and PEG-thiol ligands. The difference between the proton spectra of $HgCl_2$−PEG* and $HgCl_2$−PEG$^{\#}$ could be due to the low concentration of $HgCl_2$−PEG* or a different binding mode of

https://dx.doi.org/10.1021/acsanm.0c03134
ACS Appl. Nano Mater. 2021, 4, 1654−1663

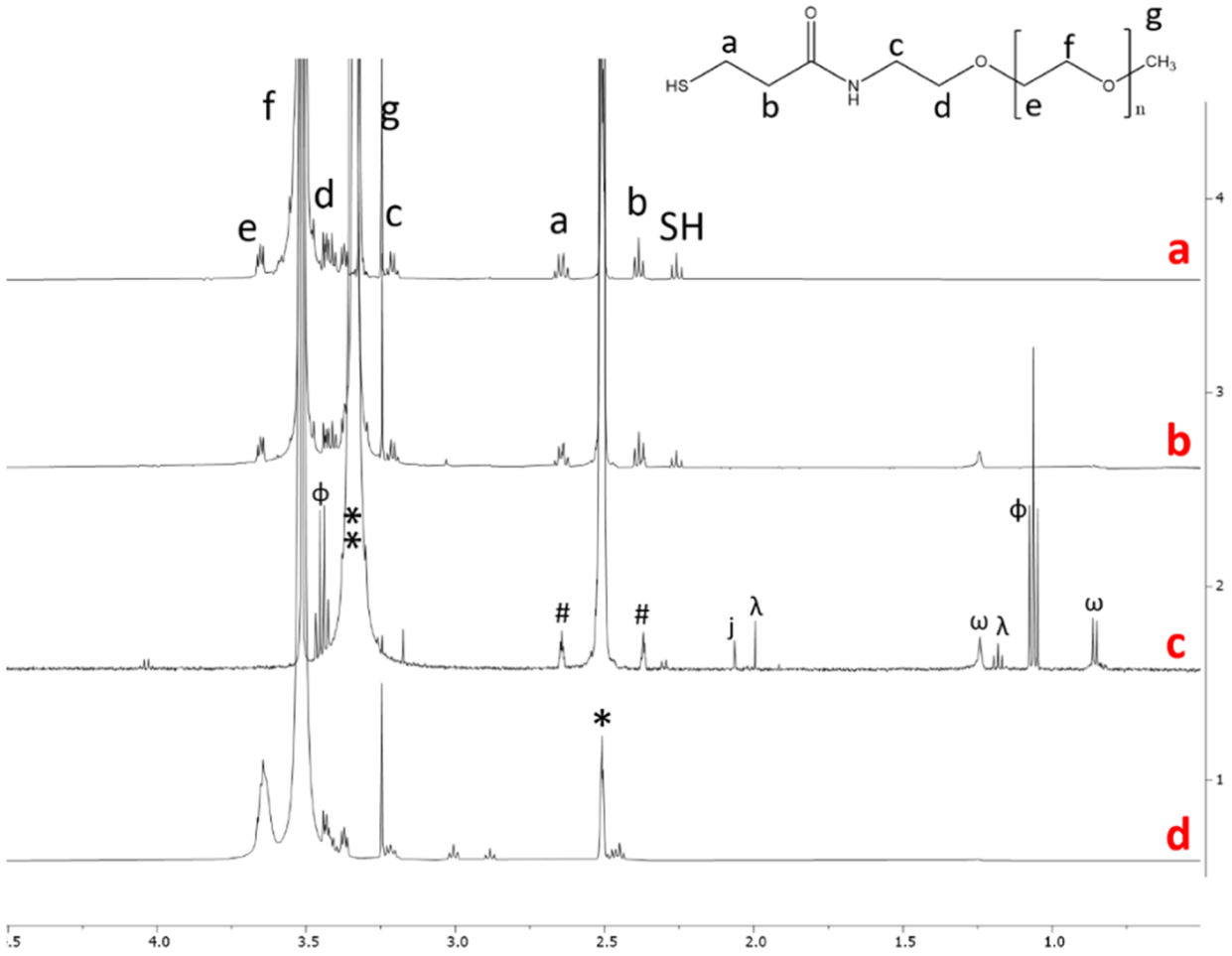

Figure 9. ^{1}H NMR spectra of (a) free PEG (20.2 mg), (b) PEG@AuNRs, (c) $HgCl_2$−PEG* obtained by adding 1.1 mg of $HgCl_2$ to PEG@AuNRs, and (d) $HgCl_2$−PEG# obtained by adding 2.0 mg of $HgCl_2$ to free PEG (43.15 mg) in DMSO-d_6. Note: * indicates DMSO-d_6 solvent, # the ^{13}C satellite from DMSO-d_6, ** the signal for HDO, and other solvent impurities indicated are *j*, acetone; *λ*, ethyl acetate; Φ, ethanol; and *ω*, grease.

the PEG-thiol ligand to the metal core. The results from the ^{1}H NMR and the evidence of precipitation (Figure S6) after [Hg^{2+}] incubation overnight give a strong indication that Hg^{2+} induced PEG-thiol ligands on the surface of AuNRs.

CONCLUSIONS

Preparation of PEG@AuNRs from CTAB@AuNRs was performed through the well-known thiol−gold chemistry approach. Due to the coating of PEG-thiol ligands, the PEG@AuNRs show superior performance compared to that of CTAB@AuNRs in a number of ways, including the sensitivity, stability, and specificity. In addition, the total number of PEG-thiol ligands on the surface of AuNRs in the sensing system can be controlled by adjusting either the concentration of AuNRs or the incubation time of PEG@AuNRs with Hg^{2+}, which detaches certain amounts of PEG-thiol from the AuNRs via Hg^{2+}−S complexation. Adjusting these inputs impacts the plasmonic responses of the system to the same concentration of mercury. The characterization of AuNR morphologies shows the differences in each sensing system. According to spectral data and AuNR shape changes obtained for various incubation times, the proposed mechanism for the adjustable sensing system includes two processes: Hg^{2+}−S complexation and amalgam formation. Evidence for this mechanism obtained from HRTEM, ^{1}H NMR, and other observations were provided. This present work enables the development of a miniature mercury plasmonic-based sensing system with an adjustable peak plasmonic response.

ASSOCIATED CONTENT

Supporting Information

The Supporting Information is available free of charge at https://pubs.acs.org/doi/10.1021/acsanm.0c03134.

Spectra of CTAB@AuNRs after amalgamation with various [Hg^{2+}]; spectra showing the change in relative absorbance of PEG@AuNRs reduced with various [Hg^{2+}]; STEM images of PEG@AuNRs after amalgamation with various concentrations of Hg^{2+} for systems with 0 and 40 min incubation time; photo of the PEG@AuNR solution incubated with $HgCl_2$ for various times; summary of ^{1}H NMR chemical shifts; and expanded image of ^{1}H NMR spectra (PDF)

AUTHOR INFORMATION

Corresponding Author

Ying Bao − *Department of Chemistry, Western Washington University, Bellingham, Washington 98225, United States;* orcid.org/0000-0001-9780-642X; Email: ying.bao@wwu.edu

https://dx.doi.org/10.1021/acsanm.0c03134
ACS Appl. Nano Mater. 2021, 4, 1654−1663

Authors

John R. Crockett − *Department of Chemistry, Western Washington University, Bellingham, Washington 98225, United States*

Hla Win-Piazza − *Department of Chemistry, Western Washington University, Bellingham, Washington 98225, United States*

Joseph E. Doebler − *Department of Chemistry, Western Washington University, Bellingham, Washington 98225, United States*

Tianqi Luan − *Department of Chemistry, Western Washington University, Bellingham, Washington 98225, United States*

Complete contact information is available at: https://pubs.acs.org/10.1021/acsanm.0c03134

Author Contributions

All authors have given approval to the final version of the manuscript.

Notes

The authors declare no competing financial interest.

■ ACKNOWLEDGMENTS

This research was supported by Western Washington University, Department of Chemistry. STEM studies were conducted on the instrument that is funded by the Joint Center for Deployment and Research in Earth Abundant Materials (JCDREAM). The authors are grateful to all the members in the Bao group for the valuable discussion. J.R.C. thanks the partial support from the RSP graduate award from Western Washington University.

■ REFERENCES

(1) Krenkel, P. A.; Goldwater, L. Mercury: Environmental Considerations, Part I. *Crit. Rev. Environ. Control* **1973**, *3*, 303−373.

(2) Clarkson, T. W.; Stockinger, H. Recent Advances in the Toxicology of Mercury with Emphasis on the Alkylmercurials. *Crit. Rev. Toxicol.* **1972**, *1*, 203−234.

(3) Rice, K. M.; Walker, E. M.; Wu, M.; Gillette, C.; Blough, E. R. Environmental Mercury and Its Toxic Effects. *J. Prev. Med. Public Health* **2014**, *47*, 74−83.

(4) Morel, F. M. M.; Kraepiel, A. M. L.; Amyot, M. The Chemical Cycle and Bioaccumulation of Mercury. *Annu. Rev. Ecol. Evol. Syst.* **1998**, *29*, 543−566.

(5) Gómez-Ariza, J. L.; Lorenzo, F.; García-Barrera, T. Comparative Study of Atomic Fluorescence Spectroscopy and Inductively Coupled Plasma Mass Spectrometry for Mercury and Arsenic Multispeciation. *Anal. Bioanal. Chem.* **2005**, *382*, 485−492.

(6) Bloom, N.; Fitzgerald, W. F. Determination of Volatile Mercury Species at the Picogram Level by Low-Temperature Gas Chromatography with Cold-Vapour Atomic Fluorescence Detection. *Anal. Chim. Acta* **1988**, *208*, 151−161.

(7) Tang, S.; Tong, P.; Lu, W.; Chen, J.; Yan, Z.; Zhang, L. A Novel Label-Free Electrochemical Sensor for Hg^{2+} Based on the Catalytic Formation of Metal Nanoparticle. *Biosens. Bioelectron.* **2014**, *59*, 1−5.

(8) Cai, S.; Lao, K.; Lau, C.; Lu, J. "Turn-on" Chemiluminescence Sensor for the Highly Selective and Ultrasensitive Detection of Hg2+ Ions Based on Interstrand Cooperative Coordination and Catalytic Formation of Gold Nanoparticles. *Anal. Chem.* **2011**, *83*, 9702−9708.

(9) Ding, Y.; Wang, S.; Li, J.; Chen, L. Nanomaterial-Based Optical Sensors for Mercury Ions. *TrAC, Trends Anal. Chem.* **2016**, *82*, 175−190.

(10) Annadhasan, M.; Muthukumarasamyvel, T.; Sankar Babu, V. R.; Rajendiran, N. Green Synthesized Silver and Gold Nanoparticles for Colorimetric Detection of Hg^{2+}, Pb^{2+}, and Mn^{2+} in Aqueous Medium. *ACS Sustain. Chem. Eng.* **2014**, *2*, 887−896.

(11) Chen, G.-H.; Chen, W.-Y.; Yen, Y.-C.; Wang, C.-W.; Chang, H.-T.; Chen, C.-F. Detection of Mercury(II) Ions Using Colorimetric Gold Nanoparticles on Paper-Based Analytical Devices. *Anal. Chem.* **2014**, *86*, 6843−6849.

(12) Zhang, Z.; Wang, H.; Chen, Z.; Wang, X.; Choo, J.; Chen, L. Plasmonic Colorimetric Sensors Based on Etching and Growth of Noble Metal Nanoparticles: Strategies and Applications. *Biosens. Bioelectron.* **2018**, *114*, 52−65.

(13) Chen, L.; Li, J.; Chen, L. Colorimetric Detection of Mercury Species Based on Functionalized Gold Nanoparticles. *ACS Appl. Mater. Interfaces* **2014**, *6*, 15897−15904.

(14) Lou, T.; Chen, Z.; Wang, Y.; Chen, L. Blue-to-Red Colorimetric Sensing Strategy for Hg^{2+} and Ag^{+} Via Redox-Regulated Surface Chemistry of Gold Nanoparticles. *ACS Appl. Mater. Interfaces* **2011**, *3*, 1568−1573.

(15) Bhattacharjee, Y.; Chatterjee, D.; Chakraborty, A. Mercapto-benzoheterocyclic Compounds Functionalized Silver Nanoparticle, an Ultrasensitive Colorimetric Probe for Hg(II) Detection in Water with Picomolar Precision: A Correlation between Sensitivity and Binding Affinity. *Sens. Actuators, B* **2018**, *255*, 210−216.

(16) Peng, C.-F.; Pan, N.; Xie, Z.-J.; Wu, L.-L. Highly Sensitive and Selective Colorimetric Detection of Hg^{2+} Based on the Separation of Hg^{2+} and Formation of Catalytic DNA−Gold Nanoparticles. *Anal. Methods* **2016**, *8*, 1021−1025.

(17) Lee, J.-S.; Han, M. S.; Mirkin, C. A. Colorimetric Detection of Mercuric Ion (Hg2+) in Aqueous Media Using DNA-Functionalized Gold Nanoparticles. *Angew. Chem., Int. Ed.* **2007**, *46*, 4093−4096.

(18) Chen, L.; Lou, T.; Yu, C.; Kang, Q.; Chen, L. N-1-(2-Mercaptoethyl)Thymine Modification of Gold Nanoparticles: A Highly Selective and Sensitive Colorimetric Chemosensor for Hg2+. *Analyst* **2011**, *136*, 4770−4773.

(19) Maity, D.; Kumar, A.; Gunupuru, R.; Paul, P. Colorimetric Detection of mercury(II) in Aqueous Media with High Selectivity Using Calixarene Functionalized Gold Nanoparticles. *Colloids Surf., A* **2014**, *455*, 122−128.

(20) Chen, L.; Fu, X.; Lu, W.; Chen, L. Highly Sensitive and Selective Colorimetric Sensing of Hg^{2+} Based on the Morphology Transition of Silver Nanoprisms. *ACS Appl. Mater. Interfaces* **2013**, *5*, 284−290.

(21) Xu, D.; Yu, S.; Yin, Y.; Wang, S.; Lin, Q.; Yuan, Z. Sensitive Colorimetric Hg^{2+} Detection Via Amalgamation-Mediated Shape Transition of Gold Nanostars. *Front. Chem.* **2018**, *6*, 566.

(22) Wang, M.; Hoff, A.; Doebler, J. E.; Emory, S. R.; Bao, Y. Dumbbell-Like Silica Coated Gold Nanorods and Their Plasmonic Properties. *Langmuir* **2019**, *35*, 16886−16892.

(23) Bao, Y.; Fong, H.; Jiang, C. Manipulating the Collective Surface Plasmon Resonances of Aligned Gold Nanorods in Electrospun Composite Nanofibers. *J. Phys. Chem. C* **2013**, *117*, 21490−21497.

(24) Chang, H.-H.; Gole, M. T.; Murphy, C. J. A Golden Time for Nanotechnology. *MRS Bull.* **2020**, *45*, 387−393.

(25) Rex, M.; Hernandez, F. E.; Campiglia, A. D. Pushing the Limits of Mercury Sensors with Gold Nanorods. *Anal. Chem.* **2006**, *78*, 445−451.

(26) Bao, Y.; Vigderman, L.; Zubarev, E. R.; Jiang, C. Robust Multilayer Thin Films Containing Cationic Thiol-Functionalized Gold Nanorods for Tunable Plasmonic Properties. *Langmuir* **2012**, *28*, 923−930.

(27) Lee, S.; Anderson, L. J. E.; Payne, C. M.; Hafner, J. H. Structural Transition in the Surfactant Layer That Surrounds Gold Nanorods as Observed by Analytical Surface-Enhanced Raman Spectroscopy. *Langmuir* **2011**, *27*, 14748−14756.

(28) Zhang, Z.; Lin, M. Fast Loading of PEG−SH on Ctab-Protected Gold Nanorods. *RSC Adv.* **2014**, *4*, 17760.

(29) Hubert, F.; Testard, F.; Spalla, O. Cetyltrimethylammonium Bromide Silver Bromide Complex as the Capping Agent of Gold Nanorods. *Langmuir* **2008**, *24*, 9219−9222.

(30) Kreke, P. J.; Magid, L. J.; Gee, J. C. 1h and 13c NMR Studies of Mixed Counterion, Cetyltrimethylammonium Bromide/Cetyltrime-

thylammonium Dichlorobenzoate, Surfactant Solutions: The Intercalation of Aromatic Counterions. *Langmuir* **1996**, *12*, 699−705.
(31) Chang, J.-Y.; Wu, H.; Chen, H.; Ling, Y.-C.; Tan, W. Oriented Assembly of Au Nanorods Using Biorecognition System. *Chem. Commun.* **2005**, 1092−1094.
(32) Mertens, S. F. L.; Gara, M.; Sologubenko, A. S.; Mayer, J.; Szidat, S.; Krämer, K. W.; Jacob, T.; Schiffrin, D. J.; Wandlowski, T. Au@Hg Nanoalloy Formation through Direct Amalgamation: Structural, Spectroscopic, and Computational Evidence for Slow Nanoscale Diffusion. *Adv. Funct. Mater.* **2011**, *21*, 3259−3267.
(33) Schulz, F.; Friedrich, W.; Hoppe, K.; Vossmeyer, T.; Weller, H.; Lange, H. Effective Pegylation of Gold Nanorods. *Nanoscale* **2016**, *8*, 7296−7308.
(34) Lin, C.-Y.; Yu, C.-J.; Lin, Y.-H.; Tseng, W.-L. Colorimetric Sensing of Silver(I) and Mercury(II) Ions Based on an Assembly of Tween 20-Stabilized Gold Nanoparticles. *Anal. Chem.* **2010**, *82*, 6830−6837.
(35) Huang, J.; Park, J.; Wang, W.; Murphy, C. J.; Cahill, D. G. Ultrafast Thermal Analysis of Surface Functionalized Gold Nanorods in Aqueous Solution. *ACS Nano* **2013**, *7*, 589−597.
(36) Wang, N.; Liu, G.; Dai, H.; Ma, H.; Lin, M. Spectroscopic Evidence for Electrochemical Effect of Mercury Ions on Gold Nanoparticles. *Anal. Chim. Acta* **2019**, *1062*, 140−146.
(37) Duan, Q.-Q.; Zhou, J.-L.; Li, P.-W.; Sun, L.; Zhuo, K.; Zhang, Y.-X.; Zhang, W.-D.; Sang, S.-B. High-Sensitivity Mercury Ion Detection System Using Unmodified Gold Nanorods. *Chin. J. Anal. Chem.* **2018**, *46*, e1874−e1879.
(38) Jin, L.-H.; Han, C.-S. Eco-Friendly Colorimetric Detection of mercury(II) Ions Using Label-Free Anisotropic Nanogolds in Ascorbic Acid Solution. *Sens. Actuators, B* **2014**, *195*, 239−245.
(39) Placido, T.; Aragay, G.; Pons, J.; Comparelli, R.; Curri, M. L.; Merkoçi, A. Ion-Directed Assembly of Gold Nanorods: A Strategy for Mercury Detection. *ACS Appl. Mater. Interfaces* **2013**, *5*, 1084−1092.
(40) Chen, L.; Lu, L.; Wang, S.; Xia, Y. Valence States Modulation Strategy for Picomole Level Assay of Hg^{2+} in Drinking and Environmental Water by Directional Self-Assembly of Gold Nanorods. *ACS Sens.* **2017**, *2*, 781−788.
(41) Yuan, A.; Wu, X.; Li, X.; Hao, C.; Xu, C.; Kuang, H. Au@Gap@Auag Nanorod Side-by-Side Assemblies for Ultrasensitive SERS Detection of Mercury and Its Transformation. *Small* **2019**, *15*, 1901958.
(42) Song, C.; Yang, B.; Zhu, Y.; Yang, Y.; Wang, L. Ultrasensitive Sliver Nanorods Array SERS Sensor for Mercury Ions. *Biosens. Bioelectron.* **2017**, *87*, 59−65.
(43) Liu, Y.; Huang, C. Z. Real-Time Dark-Field Scattering Microscopic Monitoring of the in Situ Growth of Single Ag@Hg Nanoalloys. *ACS Nano* **2013**, *7*, 11026−11034.
(44) Gu, B.; Bian, Y.; Miller, C. L.; Dong, W.; Jiang, X.; Liang, L. Mercury Reduction and Complexation by Natural Organic Matter in Anoxic Environments. *Proc. Natl. Acad. Sci. U.S.A.* **2011**, *108*, 1479−1483.
(45) Skyllberg, U.; Bloom, P. R.; Qian, J.; Lin, C.-M.; Bleam, W. F. Complexation of Mercury(II) in Soil Organic Matter: Exafs Evidence for Linear Two-Coordination with Reduced Sulfur Groups. *Environ. Sci. Technol.* **2006**, *40*, 4174−4180.
(46) Schuster, E. The Behavior of Mercury in the Soil with Special Emphasis on Complexation and Adsorption Processes - a Review of the Literature. *Water, Air, Soil Pollut.* **1991**, *56*, 667−680.
(47) Liu, D.; Qu, W.; Chen, W.; Zhang, W.; Wang, Z.; Jiang, X. Highly Sensitive, Colorimetric Detection of Mercury(II) in Aqueous Media by Quaternary Ammonium Group-Capped Gold Nanoparticles at Room Temperature. *Anal. Chem.* **2010**, *82*, 9606−9610.
(48) Thomas, K. G.; Zajicek, J.; Kamat, P. V. Surface Binding Properties of Tetraoctylammonium Bromide-Capped Gold Nanoparticles. *Langmuir* **2002**, *18*, 3722−3727.
(49) Dawson, A.; Kamat, P. V. Complexation of Gold Nanoparticles with Radiolytically Generated Thiocyanate Radicals ((Scn)2●-). *J. Mater. Chem. B* **2000**, *104*, 11842−11846.
(50) Johnson, C. J.; Dujardin, E.; Davis, S. A.; Murphy, C. J.; Mann, S. Growth and Form of Gold Nanorods Prepared by Seed-Mediated, Surfactant-Directed Synthesis. *J. Mater. Chem.* **2002**, *12*, 1765−1770.
(51) Fan, Z.; Huang, X.; Han, Y.; Bosman, M.; Wang, Q.; Zhu, Y.; Liu, Q.; Li, B.; Zeng, Z.; Wu, J.; Shi, W.; Li, S.; Gan, C. L.; Zhang, H. Surface Modification-Induced Phase Transformation of Hexagonal Close-Packed Gold Square Sheets. *Nat. Commun.* **2015**, *6*, 6571.
(52) Diroll, B. T.; Schaller, R. D. Shape-Selective Optical Transformations of Cdse Nanoplatelets Driven by Halide Ion Ligand Exchange. *Chem. Mater.* **2019**, *31*, 3556−3563.
(53) Antanovich, A.; Achtstein, A. W.; Matsukovich, A.; Prudnikau, A.; Bhaskar, P.; Gurin, V.; Molinari, M.; Artemyev, M. A Strain-Induced Exciton Transition Energy Shift in Cdse Nanoplatelets: The Impact of an Organic Ligand Shell. *Nanoscale* **2017**, *9*, 18042−18053.
(54) Guo, C.; Yarger, J. L. Characterizing Gold Nanoparticles by NMR Spectroscopy. *Magn. Reson. Chem.* **2018**, *56*, 1074−1082.
(55) Hens, Z.; Martins, J. C. A Solution NMR Toolbox for Characterizing the Surface Chemistry of Colloidal Nanocrystals. *Chem. Mater.* **2013**, *25*, 1211−1221.
(56) Hong, Y.; Lee, E.; Choi, J.; Oh, S. J.; Haam, S.; Huh, Y.-M.; Yoon, D. S.; Suh, J.-S.; Yang, J. Gold Nanorod-Mediated Photothermal Modulation for Localized Ablation of Cancer Cells. *J. Nanomater.* **2012**, *2012*, 825060.
(57) Mahmoud, N. N.; Alhusban, A. A.; Ali, J. I.; Al-Bakri, A. G.; Hamed, R.; Khalil, E. A. Preferential Accumulation of Phospholipid-Peg and Cholesterol-Peg Decorated Gold Nanorods into Human Skin Layers and Their Photothermal-Based Antibacterial Activity. *Sci. Rep.* **2019**, *9*, 5796.
(58) Schuetze, B.; Mayer, C.; Loza, K.; Gocyla, M.; Heggen, M.; Epple, M. Conjugation of Thiol-Terminated Molecules to Ultrasmall 2nm Gold Nanoparticles Leads to Remarkably Complex 1h-NMR Spectra. *J. Mater. Chem. B* **2016**, *4*, 2179−2189.
(59) Qian, H.; Zhu, M.; Gayathri, C.; Gil, R. R.; Jin, R. Chirality in Gold Nanoclusters Probed by NMR Spectroscopy. *ACS Nano* **2011**, *5*, 8935−8942.
(60) Gautier, C.; Bürgi, T. Chiral Gold Nanoparticles. *ChemPhysChem* **2009**, *10*, 483−492.
(61) Noguez, C.; Garzón, I. L. Optically Active Metal Nanoparticles. *Chem. Soc. Rev.* **2009**, *38*, 757−771.

https://dx.doi.org/10.1021/acsanm.0c03134
ACS Appl. Nano Mater. 2021, 4, 1654−1663